

Interaction between two parallel fire fronts under different wind conditions

Carlos Ribeiro^{A,*} , Luís Reis^A, Jorge Raposo^A, André Rodrigues^A, Domingos Xavier Viegas^A and Jason Sharples^{B,C}

For full list of author affiliations and declarations see end of paper

***Correspondence to:**

Carlos Ribeiro
Univ Coimbra, ADAL, Departamento de Engenharia Mecânica, Rua Luís Reis Santos, Pólo II, 3030-788 Coimbra, Portugal
Email: carlos.ribeiro@adai.pt

Received: 24 August 2021

Accepted: 13 March 2022

Published: 20 May 2022

Cite this:

Ribeiro C *et al.* (2022)
International Journal of Wildland Fire
31(5), 492–506. doi:[10.1071/WF21120](https://doi.org/10.1071/WF21120)

© 2022 The Author(s) (or their employer(s)). Published by CSIRO Publishing on behalf of IAWF. This is an open access article distributed under the Creative Commons Attribution-NonCommercial-NoDerivatives 4.0 International License ([CC BY-NC-ND](https://creativecommons.org/licenses/by-nc-nd/4.0/))

OPEN ACCESS

ABSTRACT

Wildfires often exhibit complex and dynamic behaviour arising from interactions between the fire and surrounding environment that can create a rapid fire advance and result in loss of containment and critical fire safety concerns. A series of laboratory experiments involving the interaction of two parallel fire lines on a uniform fuel bed without slope under the influence of wind is presented and discussed. The two fire lines are initially separated by a certain distance (1, 2 m) and the subsequent fire spread is described. The results show that the pyroconvective interaction between the two fire lines and ambient wind modified the rate of spread of the approaching fire lines and their associated spread characteristics, independently of the distance between them. A physical interpretation of fire evolution based on the dynamic interaction between two parallel fire lines under wind flow is proposed. We use a dimensionless physical parameter, the Froude number. The results also demonstrated the existence of a wind flow velocity between 1 and 2 m s⁻¹, corresponding to a Froude number between 0.2 and 0.4 for which the rate of approach of the two merging fire lines is a minimum.

Keywords: accelerating fires, convergent fire fronts, dynamic fire behaviour, extreme fire behaviour, fire behaviour, forest fires, merging fires, parallel fronts.

Introduction

Wildfire propagation is a complex phenomenon that is not fully understood. Over the last several decades, wildfire behaviour researchers have employed empirical and theoretical analyses with the main objective of predicting fire behaviour in the landscape. [Pastor *et al.* \(2003\)](#) and [Sullivan \(2009\)](#) provide a survey of this effort illustrating the complexity of the problem. Nowadays, it is possible to predict fire behaviour under a very limited set of conditions ([Thomas *et al.* 2017](#)), but beyond such conditions, predictive capability can be severely compromised. For example, fires burning under extreme conditions, which burn with great intensity and are subject to dynamic interactions between the fire and the surrounding environment, remain beyond the realms of reliable prediction. These fires can exhibit abrupt, rapid and unexpected changes in fire behaviour that endanger people's lives and defy suppression efforts ([Bowman *et al.* 2017](#)).

The interaction of fires has been observed and studied by several authors. [Brown and Davis \(1973\)](#) noted that during prescribed burning, the fire fronts or even some parts of the fire near the plot edges are dangerous because runs with the highest rates of spread (ROS) on one side of the plot may develop, and the fire can jump out of the plot and a spot fire can occur. [Johansen \(1984\)](#) observed that in prescribed fires, the merging of spot fires caused a rapid spread of the fire and an increase in flame length, while [Pyne \(1984\)](#) noted that large fires attract small fires and multiple heads can burn out the intervening fuels and merge. [Clark *et al.* \(1996\)](#) highlighted the importance and the utility of developing a coupled atmosphere–fire model based on the basic equations of motion and thermodynamics and demonstrated the convergence pattern in the vicinity of linear fire lines as a result of air being drawn into the fire's hot air column. In the absence of ambient wind and slope, a vertically oriented convective cell draws in low-level air

equally from all sides. In the presence of wind, this dynamic is modified in a way that results in the evolution of the parabolic or conical shape of the fire line.

Morvan (2007) developed a numerical study to analyse the flame geometry and the potential for crown fire for wildfires propagating through shrubland fuels, and introduced a dimensionless physical parameter, the Froude number (Fr), that can be defined by the ratio between the inertial force due to the wind flow and buoyancy. He considered that, when the wind flow is less than 6 m s^{-1} , the flame length increases, but beyond this value, if wind velocity increases, a sharp reduction in flame length is observed. He explained that this phenomenon can be related to the buoyancy flow due to the vertical expansion of the hot gases above the combustion zone and the inertial flow induced by the wind, and the ratio of these two forces can be represented using the dimensionless physical parameter, the Froude number.

Sullivan (2007) used a set of experimental field tests, conducted in the Northern Territory, Australia, in July and August 1986, to analyse the role of the convective Froude number and Byram's energy criterion. He found that Byram's energy criterion can be calculated as the inverse cube of the convective Froude number. Byram's energy criterion (or the Byram number) is another non-dimensional physical parameter that relates the horizontal dynamic force produced by the wind flow and the vertical buoyant forces of the fire. However, Clark *et al.* (1996), Morvan (2007) and Sullivan (2007) consider only one linear fire line propagating perpendicular to the wind.

Viegas *et al.* (2012) studied the interaction and merging of two oblique and symmetric fire fronts that intersect at a single point (forming a 'V'-shaped fire line) and developed a conceptual analytical model for the ROS of the vertex of the 'V'. The merging of two fire fronts intersecting at a single point has been analysed by several authors during the last decade and this phenomenon has been described as a 'junction fire' (Sharples *et al.* 2013; Viegas *et al.* 2013a; Raposo *et al.* 2015, 2018; Sullivan *et al.* 2019). Recently, Filkov *et al.* (2020) developed a simple, fast and accurate method to track fire front propagation and quantify merging fire behaviour at field scales.

Morvan *et al.* (2011) numerically analysed the interaction between two parallel fire fronts using a flat grassland fuel bed, and a wind direction perpendicular to the fire lines, so that the propagation of fire was in opposite directions (one fire spreading as a head fire and the other as a back fire). This analysis was intended to reproduce the behaviour that can occur during fire suppression operations (i.e. 'backburning'). They concluded that the interaction occurs only at a fairly short distance. In our literature survey, we did not find any study addressing the problem of two parallel fire lines under different wind conditions such as those analysed in the present paper.

Fig. 1 shows the estimated fire perimeter of wildfires that occurred in Quiaios, Portugal, on 15 October 2017. The first ignition happened in Quintã at 13:34 hours (see orange star

in Fig. 1), and the main ignition occurred in Cova de Serpe 1 h later; in Fig. 1, the yellow star represents the approximate location of this ignition. The Cova de Serpe ignition produced a spot fire that spread parallel to the main fire under strong wind conditions on flat ground (cf. Viegas *et al.* 2019); in Fig. 1, the green star represents the approximate location of this spot fire. According to ground and aerial photos, the flanks of these fires spread for at least 7 km while remaining at a distance of 200 m apart before eventually merging – the orange region with ref. no. 20171015_1800 in Fig. 1 represents the estimated position of this fire perimeter between 16:00 and 18:00 hours. The present study aims to describe the process of two fire lines merging under a wind flow blowing parallel to the lines of fire, a process that is not well understood or even studied.

Physical problem

In the present study, it is assumed that two parallel fire lines are spreading on flat terrain and can interact with each other under the influence of wind flow. The two fire lines are separated initially by a distance d on a uniform fuel bed, as illustrated schematically in Fig. 2a. The Cartesian coordinate system $O_oX_oY_oZ_o$ is considered, in which O_oZ_o is perpendicular to the ground. The study area is defined by $ABCD$ and the fuel bed area is defined by $EFGH$. Line EF is shifted (1 m) in the O_oX_o axis. The fuel bed area is covered by a uniform layer of forest fuel able to support the spread of a surface fire.

We consider two linear fire fronts, each 2 m in length, defined by two straight lines (IJ and KL), symmetric in the OXZ plane, with a distance d between them, as shown in Fig. 2a. Henceforth, the linear fire lines IJ and KL will be referred to as l_1 and l_2 , respectively. A uniform boundary layer-type flow is blowing parallel to the OX_o axis with a characteristic velocity (U_0), represented by black arrows in Fig. 2a. At time $t_0 = 0 \text{ s}$, the fire lines are ignited and are free to spread in all directions.

Material and methods

Laboratory experiments

The experimental study was carried out at the Combustion Tunnel (CT) of the Forest Fire Research Laboratory of the University of Coimbra in Lousã (Portugal). The CT has a working area of $6 \times 8 \text{ m}^2$, defined by $ABCD$ in Fig. 2a. The fuel bed area was $4 \times 5 \text{ m}^2$, with side dimensions EF and GH of 4 m and, the other sides, FG and EH , of 5 m. To avoid boundary effects inside the wind CT, a gap of 1 m between the vertical walls of the combustion tunnel and the edges of the fuel bed (EF and GH) was left. The wind flow was produced by two fans with maximum power and flow velocity of 70 kW and 8 m s^{-1} , respectively. The tests were performed with reference wind velocities of 0, 1, 2, 3, 4 and 5 m s^{-1} . The reference wind velocity (U_0) was measured

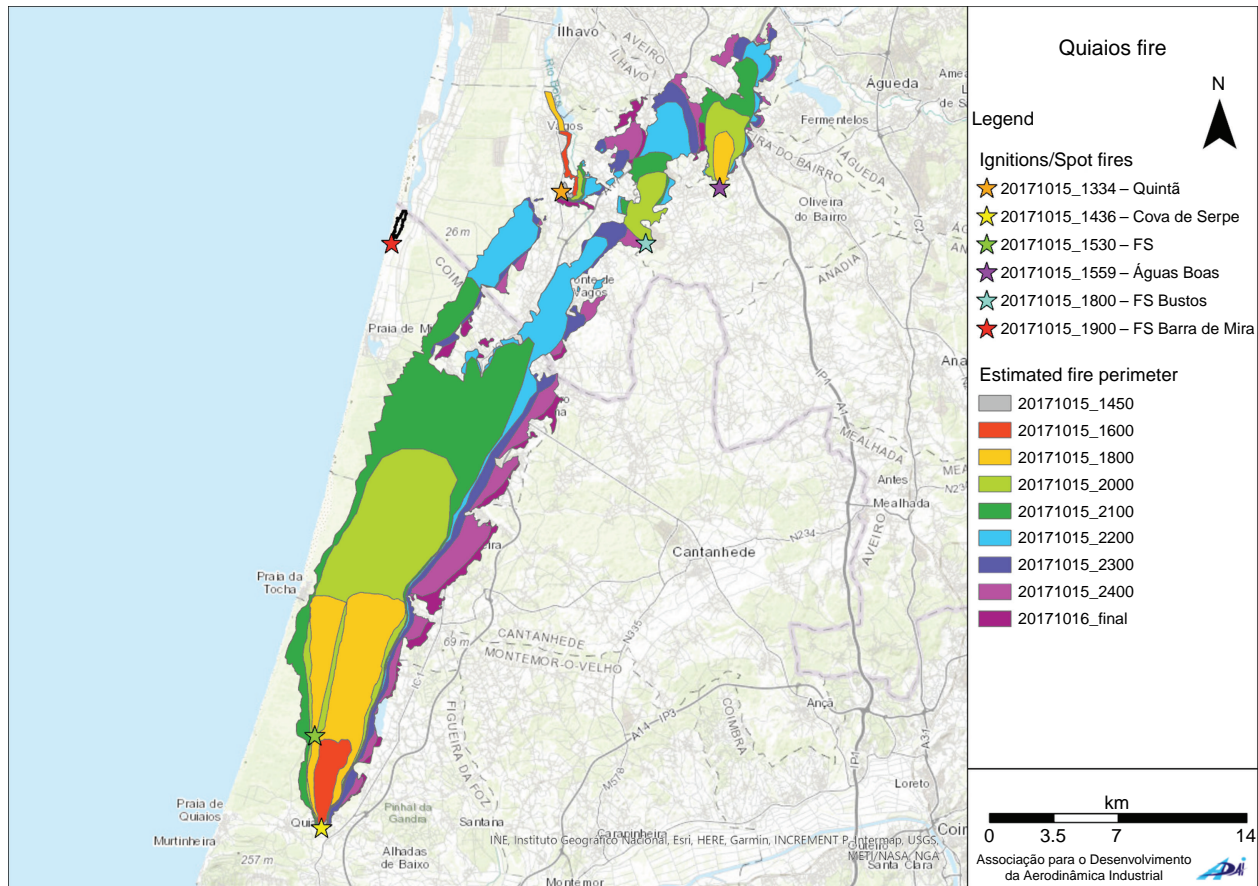


Fig. 1. Estimated fire perimeter of the Quiaios wildfires on 15 October 2107. The stars and the coloured surfaces represent the ignitions/spot fires that happened in this complex Quiaios wildfire and the estimated fire perimeter during the time, respectively. The yellow star represents the approximate location of the main ignition in Cova de Serpe – Quiaios at 14:36 hours. The green star represents the spot fire at 15:30 hours. The orange region is the estimated burned area between 16:00 and 18:00 hours, and for approximately 7 km, the main fire and the spot fire spread in parallel.

in the *OX* axis with a KimoAMI 300 hot-wire probe (Kimo Instruments, Montpon-Ménéstérol, France) 22 cm above the CT floor. More details can be seen in Fig. A1.

During the preparation of each test, the conditions of the fuel load and bulk density were controlled, and the air temperature ($^{\circ}\text{C}$), relative humidity (%) and fuel moisture (m_f) were monitored. The fuel bed for the experiments was composed of dry particles of straw (*Avena sativa*) with a constant load of 600 g m^{-2} (dry basis). The fuel bed height (h_f) was measured at five random positions and on average was 0.07 m, and the packing ratio (β_f), given by the ratio of the fuel bed bulk density (ρ_b) to the fuel particle density (ρ_p), was 0.029 (Viegas and Pita 2004; Xie et al. 2014; Raposo 2016; Raposo et al. 2018; Rodrigues et al. 2019). The fuel properties are approximately: particle surface-area-to-volume ratio (σ_f) 4734 m^{-1} ; bulk density (ρ_b) 7.5 kg m^{-3} ; fuel particle density (ρ_p) 258 kg m^{-3} and high heat of combustion (HHC) 18 kJ kg^{-1} (Catchpole et al. 1993; Almeida 2005; Águeda et al. 2011). The fuel moisture content was measured twice for each test with an A&D ML50 moisture analyser:

during preparation of the fuel bed and before ignition for each test. To ensure that the moisture content of the fuel in contact with ambient air did not change, the time between the preparation of the fuel bed and the beginning of the burn test did not exceed 10 min. The basic ROS R_o (cm s^{-1}) of a linear fire front in a fuel bed with the same properties was measured for each series of tests using a $1 \times 1\text{ m}^2$ horizontal fuel bed without wind. The corresponding values are given in Table 1. The ignition of the two fire lines (lines l_1 and l_2) was made by two persons to ensure that the lines started burning simultaneously. For this purpose, two wool threads soaked in a mixture of petrol (50%) and diesel fuel (50%) were used.

The tests were monitored and recorded with an infrared camera (FLIR SC660) and a video camera in the visible range. The parameters considered for the infrared camera were a temperature range between 300 and 1500°C , an emissivity value of 0.98 (Dlugogorski et al. 2014) and an acquisition rate of 15 Hz. A threshold of 350°C was used to avoid obstruction of the view by the plume of the fire. The two cameras were placed at the top of the lifting

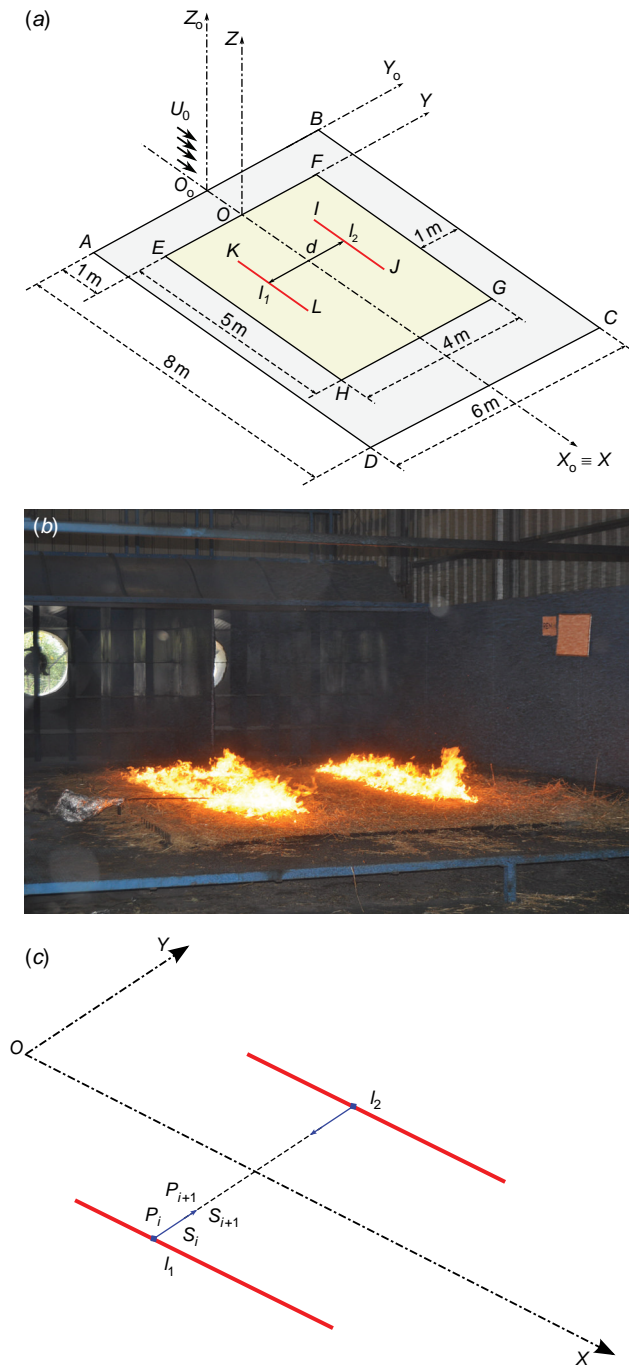


Fig. 2. (a) Geometry of two parallel fire lines in symmetrical conditions. (b) View of the combustion tunnel (CT) of the Forest Fire Laboratory of the University of Coimbra. (c) Evaluation of the ROS of the approaching two parallel fires lines.

platform, shown top-left of Fig. 3, and each recording was in continuous mode. In order to avoid parallax errors, the angle between the infrared camera optical axis and the ground surface of the CT was approximately 90°. In order to reduce uncertainty, three replicate tests (T1, T2 and T3) were performed for each set of parameters, as shown in Table 1.

The infrared videos were used to obtain the fire contour perimeter at pre-defined times. The time between frames was adjusted for each test and was used to calculate the ROS of the interaction between the fire fronts. To determine the evolution of the fire front, the Cartesian coordinates of the frame points were used to calculate the instantaneous values of ROS at each point of the fire line. More details can be seen in Raposo *et al.* (2018) and Rodrigues *et al.* (2019). The interaction between the two fire lines was analysed along three reference lines (lines a, b and c), at a distance of 1.0, 1.5 and 2.0 m in relation to the OXYZ reference frame, measured in the OX axis. As an example, in Fig. 4, the isochrones of one of the tests (1-D₁U₃) are shown together with the reference lines that were used to analyse the fire spread.

Evaluation of the ROS of the approaching fires

The evaluation of the instantaneous ROS of the approaching lines (see Fig. 2a, c) is measured along each reference line a, b and c, according to Fig. 4. If P_i and P_{i+1} are the positions of the fire line along the reference line and S_i and S_{i+1} are the distances travelled by the fire line from the origin, then we estimate the instantaneous value R_j of the ROS in the OY direction with:

$$R_j = \frac{\Delta S_i}{\Delta t_i} = \frac{s_{i+1} - s_i}{t_{i+1} - t_i} \quad (1)$$

We calculate this value for time t_j and at distance S_j given by:

$$t_j = \frac{t_i + t_{i+1}}{2} \quad (2)$$

$$S_j = \frac{S_i + S_{i+1}}{2} \quad (3)$$

As we intend to correlate the fire properties with R_j , they will be determined for the corresponding time t_j for each time step. In the present study, in order to minimise the effect of the fuel moisture content m_f on R_j , we use the non-dimensional ROS (Viegas 2006) calculated from:

$$R' = \frac{R_j}{R_o} \quad (4)$$

where R_o represents the basic ROS (cm s^{-1}) under no-slope and no-wind conditions. The basic ROS R_o is an intrinsic property of the fuel bed and depends mainly on the moisture content m_f of the fuel particles (Catchpole *et al.* 2001; Martins Fernandes 2001; Alexander and Cruz 2013; Viegas *et al.* 2013b; Lopes *et al.* 2014; Xie *et al.* 2020).

In order to compare the results obtained for different values of initial separation d , we introduce a non-dimensional distance (S'), defined by:

$$S' = \frac{S_j}{d} \quad (5)$$

Table 1. Parameters of the parallel fire fronts under wind conditions.

Ref.	d (m)	U ($m\ s^{-1}$)	Designation			m_f (%)			R_o ($cm\ s^{-1}$)		
			T1	T2	T3	T1	T2	T3	T1	T2	T3
1	1	0	I-D ₁ U ₀	2-D ₁ U ₀	3-D ₁ U ₀	9.1	9.0	9.3	0.83	0.85	0.81
2		1	I-D ₁ U ₁	2-D ₁ U ₁	3-D ₁ U ₁	10.2	10.4	10.7	0.70	0.75	0.72
3		2	I-D ₁ U ₂	2-D ₁ U ₂	3-D ₁ U ₂	9.5	9.5	9.5	0.85	0.85	0.85
4		3	I-D ₁ U ₃	2-D ₁ U ₃	3-D ₁ U ₃	10.4	10.2	10.7	0.75	0.70	0.74
5		4	I-D ₁ U ₄	2-D ₁ U ₄	3-D ₁ U ₄	10.8	10.9	10.9	0.71	0.72	0.72
6		5	I-D ₁ U ₅	2-D ₁ U ₅	3-D ₁ U ₅	11.2	11.1	11.3	0.60	0.61	0.64
7	2	0	I-D ₂ U ₀	2-D ₂ U ₀	3-D ₂ U ₀	10.0	9.5	9.7	0.76	0.80	0.76
8		1	I-D ₂ U ₁	2-D ₂ U ₁	3-D ₂ U ₁	10.0	10.2	10.1	0.77	0.75	0.77
9		2	I-D ₂ U ₂	2-D ₂ U ₂	3-D ₂ U ₂	10.0	10.2	10.1	0.77	0.75	0.77
10		3	I-D ₂ U ₃	2-D ₂ U ₃	3-D ₂ U ₃	9.5	9.4	9.5	0.80	0.83	0.80
11		4	I-D ₂ U ₄	2-D ₂ U ₄	3-D ₂ U ₄	11.2	11.1	11.3	0.65	0.67	0.65
12		5	I-D ₂ U ₅	2-D ₂ U ₅	3-D ₂ U ₅	10.8	10.9	10.9	0.71	0.70	0.71



Fig. 3. General view of the combustion tunnel of the Forest Fire Research Laboratory of the University of Coimbra. The length of the working section is 8 m and the width is 6 m. The maximum flow velocity is $8\ m\ s^{-1}$. The position of the infrared camera and the visible camera can be seen at the top left of the image, on the lifting platform.

where d is the pre-determined separation of the two fire lines (1 or 2 m). This analysis was made in both positive and negative OY directions. Assuming that the fire is spreading symmetrically, the average of the two values is taken to characterise each time step.

Balance between horizontal and vertical forces

The physical problem analysed in our work is related to the horizontal force provided by the wind flow and the vertical forces associated with the fire-induced buoyancy. We use the non-dimensional convective Froude number, Fr , to describe the ratio between these two forces, defined by:

$$Fr = \sqrt{\frac{U_0^2}{g \times L}} \tag{6}$$

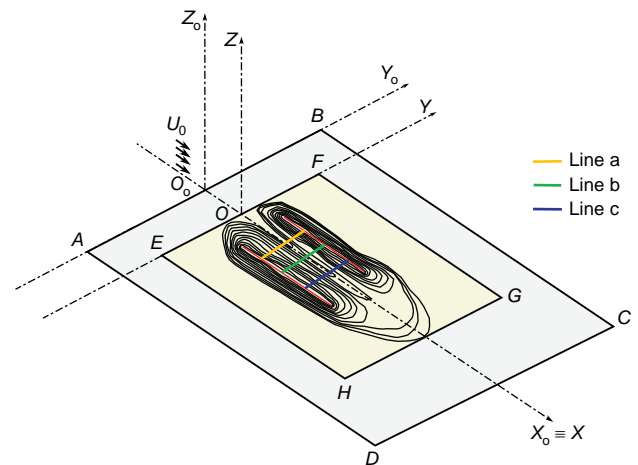


Fig. 4. Measurement directions of the fire propagation with lines a, b and c. The isochrones correspond to test I-D₁U₃ ($d = 1\ m$ and $U = 3\ m\ s^{-1}$).

where U_0 is reference wind velocity ($m\ s^{-1}$), g is acceleration due to gravity ($9.81\ m\ s^{-2}$) and L (m) is a length that characterises the size of the combustion area producing buoyancy. To estimate this parameter, we considered two options: (i) the average length $L(t_j)$ of the two fire lines measured along the OX axis at each time step; (ii) the square root of the burned area $A(t_j)$ of each fire line at each time step.

The average value of two fire line lengths l_1 and l_2 along the OX axis is defined by:

$$L(t_j) = \frac{L_{l1}(t_j) + L_{l2}(t_j)}{2} \tag{7}$$

where t_j is the time step defined in Eqn 2.

The square root of the average value of the two fire line areas is defined by:

$$L^*(t_j) = \sqrt{\frac{A_{l1}(t_j) + A_{l2}(t_j)}{2}} = \sqrt{\frac{c_1 \cdot L_{l1}(t_j) \cdot B_{l1}(t_j) + c_2 \cdot L_{l2}(t_j) \cdot B_{l1}(t_j)}{2}} \quad (8)$$

In this equation, B_{li} is the width of each burned area and c_i is a shape coefficient, which is equal to 1 if we assume that the shape of the fire is a rectangle.

The vertical forces associated with the Froude number were analysed with the two approaches: the fire length L and the square root of the burnt area L^* . The values that we obtained were not significantly different and, for this reason, we used L , because it is easier to obtain.

Statistical analysis

In order to reduce uncertainty, three replicates (T1, T2 and T3) were performed for each set of parameters, as shown in Table 1 and all results presented in this study are the average of the three replicates. The error bars and the dashed line curves in the figures represent the $\pm 95\%$ confidence intervals.

We consider that the approaching ROS of two linear fire lines can be influenced by the wind flow (U_0), which changes the flame geometry, the horizontal and vertical forces resulting from the wind flow and the vertical buoyant of the fire, respectively, and the gap distance (d) between the two fire lines. In order to check the combined influence of each variable, an analysis of variance (ANOVA) was carried out to test for the effects of the wind flow velocity ($U_0 = 0, 1, 2,$

3 and 5 m s^{-1}) and the distance between the parallel fire lines ($d = 1$ and 2 m). ANOVA is a statistical method for determining the existence of differences among several population means, which requires the analysis of different forms of variance associated with the random samples under study (see e.g. Devore 2010).

Results and discussion

Rate of spread analysis

When the fire lines are ignited, initially they are segments of a straight line, but when they spread under the influence of wind flow (horizontal forces) and buoyancy flow (vertical forces), they become curved and the spreading conditions may change along the OX axis with the development of the fire. Based on general observations of fire behaviour (IR camera, visual [ocular] and colour video observations) during the experiments, there was a large change on fire dynamics when the wind flow velocity (U_0) was increased in comparison with the effect of changing the distance between the fronts (d).

In order to assess these dynamic changes, in each test we estimated the instantaneous value R_j for each reference line (lines a, b and c; Fig. 4) every 5 s from fire perimeter plots obtained with the IR camera. The non-dimensional instantaneous or local ROS R' was calculated according to Eqn 4. The basic ROS (R_0) for each set of parameters can be seen in Table 1. The average, minimum, maximum and s.d. values of non-dimensional ROS (R') for the three experiments (T1, T2 and T3) and for each reference line (lines a, b and c) were calculated and are given in Table 2.

Table 2. Summary of the non-dimensional ROS (R'_j) for experiments at three reference lines (lines a, b and c).

Ref	d (m)	U (m s^{-1})	R'_j for reference lines a, b and c		
			R'_a	R'_b	R'_c
1	1	0	3.60 (2.77–4.42, 0.64)	3.64 (2.07–5.26, 0.92)	3.79 (2.57–4.64, 0.74)
2		1	1.84 (1.16–3.24, 0.58)	1.93 (1.15–3.12, 0.55)	2.24 (1.06–4.27, 0.83)
3		2	1.76 (1.33–2.39, 0.34)	2.17 (1.27–3.06, 0.54)	2.11 (1.55–3.06, 0.55)
4		3	2.16 (1.29–2.95, 0.49)	2.41 (1.21–4.72, 1.27)	2.38 (1.24–4.09, 0.85)
5		4	2.41 (0.73–3.80, 0.85)	2.77 (1.86–3.83, 0.66)	2.58 (1.49–3.73, 0.69)
6		5	3.15 (1.50–5.02, 1.10)	3.18 (1.60–5.46, 1.33)	3.31 (1.05–6.82, 1.54)
7	2	0	3.29 (1.55–4.89, 0.98)	3.64 (2.42–5.66, 1.04)	3.23 (1.54–5.29, 1.00)
8		1	1.95 (1.26–3.17, 0.52)	1.99 (0.77–3.61, 0.75)	2.41 (1.40–3.47, 0.54)
9		2	1.81 (1.21–2.87, 0.46)	1.82 (1.13–3.47, 0.65)	2.11 (1.52–2.77, 0.43)
10		3	2.22 (0.61–3.20, 0.70)	2.16 (1.64–3.19, 0.47)	1.94 (1.20–2.78, 0.42)
11		4	2.46 (1.53–4.28, 0.82)	2.76 (1.20–3.87, 0.78)	2.88 (0.62–4.64, 1.08)
12		5	4.27 (1.30–9.21, 2.10)	4.11 (0.94–8.04, 1.97)	3.77 (2.42–6.23, 1.20)

Values in table consist of average (min.–max., s.d.). An R'_j of 3, for example, equates to the experiments having 3 times the ROS of the basic ROS (R_0 : ROS no wind and no slope).

For the two fire lines at an initial distance $d = 1$ m, for all wind flow intervals considered, the average of non-dimensional ROS values ranged between 1.76 ($U_0 = 2 \text{ m s}^{-1}$) and 3.79 ($U_0 = 0 \text{ m s}^{-1}$). In contrast, for the two fire lines at an initial distance $d = 2$ m, the average ranged between 1.81 ($U_0 = 2 \text{ m s}^{-1}$) and 4.11 ($U_0 = 5 \text{ m s}^{-1}$) (Table 2). For each unique set of conditions tested, the non-dimensional ROS was generally largest for wind flow equal to $U_0 = 0$ and 5 m s^{-1} , and lowest for the wind flow $U_0 = 1$ and 2 m s^{-1} (see Table 2).

However, for clarity, in the following figures, we represent the mean of the results for the three repetitions run under the same conditions. The fire spread can be described as a function of either time or space (distance) (cf. Viegas et al. 2021); from now on, we use non-dimensional distance to analyse the evolution of the ROS of the two approaching fires, as this gives a better indication of the fire behaviour, as the distance between the fire lines is reduced to zero as S' tends to 0.5.

In Fig. 5, the non-dimensional average ROS $R'_{\ell\text{ave}}$ values for each reference line a, b or c, with the configuration mentioned before, are plotted as a function of the non-dimensional distance S' . As can be seen, there no marked difference between the three lines in each test configuration and the average local ROS R'_{ave} values for the three lines a, b and c can be used to estimate the local behaviour of the approaching fire lines for each set of values of d and U_0 . We used the same methodology as Viegas et al. (2021).

In Fig. 6, the average of the non-dimensional values of local ROS R'_{ave} with standard deviation bars (corresponding to 95% confidence intervals) are plotted as a function of the non-dimensional distance S' for two tests performed with $d = 1$ and 2 m for each wind velocity value, $U_0 = 0, 1, 2, 3, 4$ and 5 m s^{-1} .

The behaviour of the approaching fires is non-monotonic (Viegas et al. 2021) in the sense that it is not constant and, on the contrary, the laterally spreading fire tends to decelerate or accelerate. Our results indicate that for both values of d considered, the behaviour is less dependent on the initial distance and more dependent on the ambient wind velocity, because the combination of wind flow velocity and buoyancy flow changes the approaching fires and dynamic fire behaviour.

We now present the results of the approaching fires along the OY axis that illustrate the changing behaviour of fire spread when the flow velocity is modified.

As shown in Fig. 6a ($U_0 = 0 \text{ m s}^{-1}$), the value of R' has two stages: first when $S' \sim 0-0.25$, the R'_{ave} increases, because the flames lean over towards each other; then, the flames become more vertical and their length and height increase. After this, R'_{ave} decreases until $S' \sim 0.5$ because the flames are leaning over towards the burned area and the flames' length and height continue to decrease. The convective process between two fire lines during the first stage induces an acceleration during the approach of the fire; however, when the burned area increases, this convective process changes and a deceleration phase occurs.

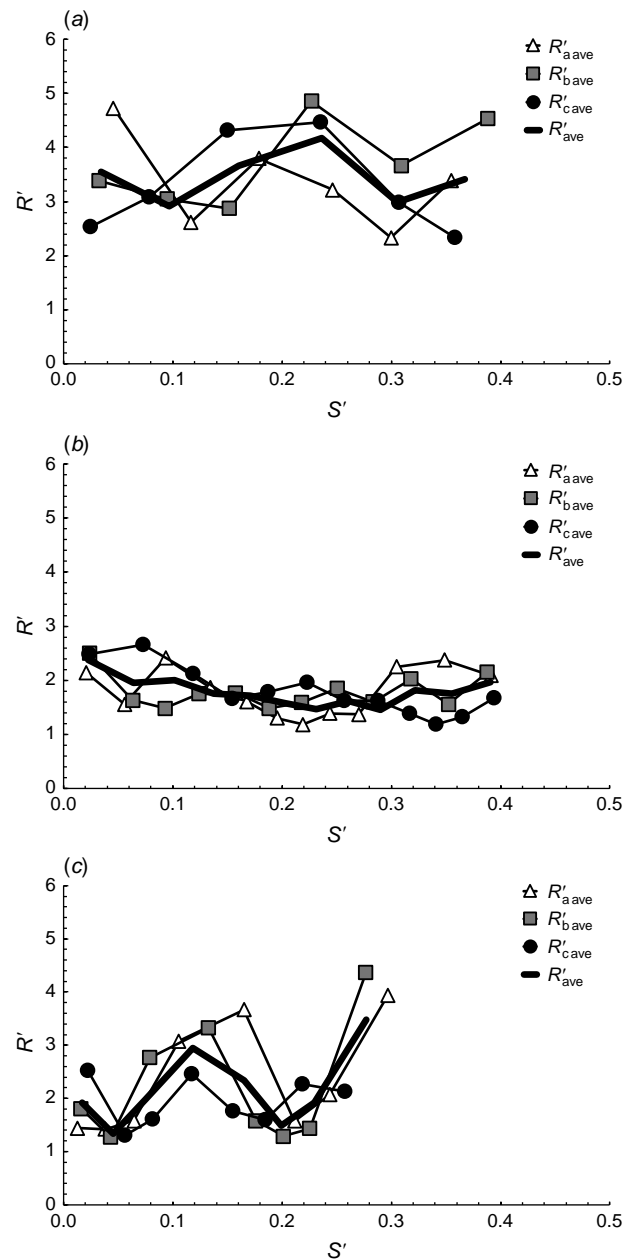


Fig. 5. Non-dimensional average ROS $R'_{\ell\text{ave}}$ values for each reference line a, b or c as a function of the non-dimensional distance S' , together with the average ROS R'_{ave} values. The fire fronts distance is $d = 2$ m. (a) $U_0 = 0 \text{ m s}^{-1}$; (b) $U_0 = 2 \text{ m s}^{-1}$; (c) $U_0 = 5 \text{ m s}^{-1}$.

For $U_0 = 1 \text{ m s}^{-1}$ (Fig. 6b), the value of R'_{ave} has a relatively high initial value, less than R' for $U_0 = 0 \text{ m s}^{-1}$, but during the approaching fires, when S' increases, the R' value decreases.

However, for $U_0 = 2 \text{ m s}^{-1}$ (Fig. 6c for this experimental setting), the approaching velocity is relatively constant. For both wind flow velocities ($U_0 = 1$ and 2 m s^{-1}), the convection flow is symmetrical on both sides of each fire front. In that case, the wind inhibits the interaction and the flames

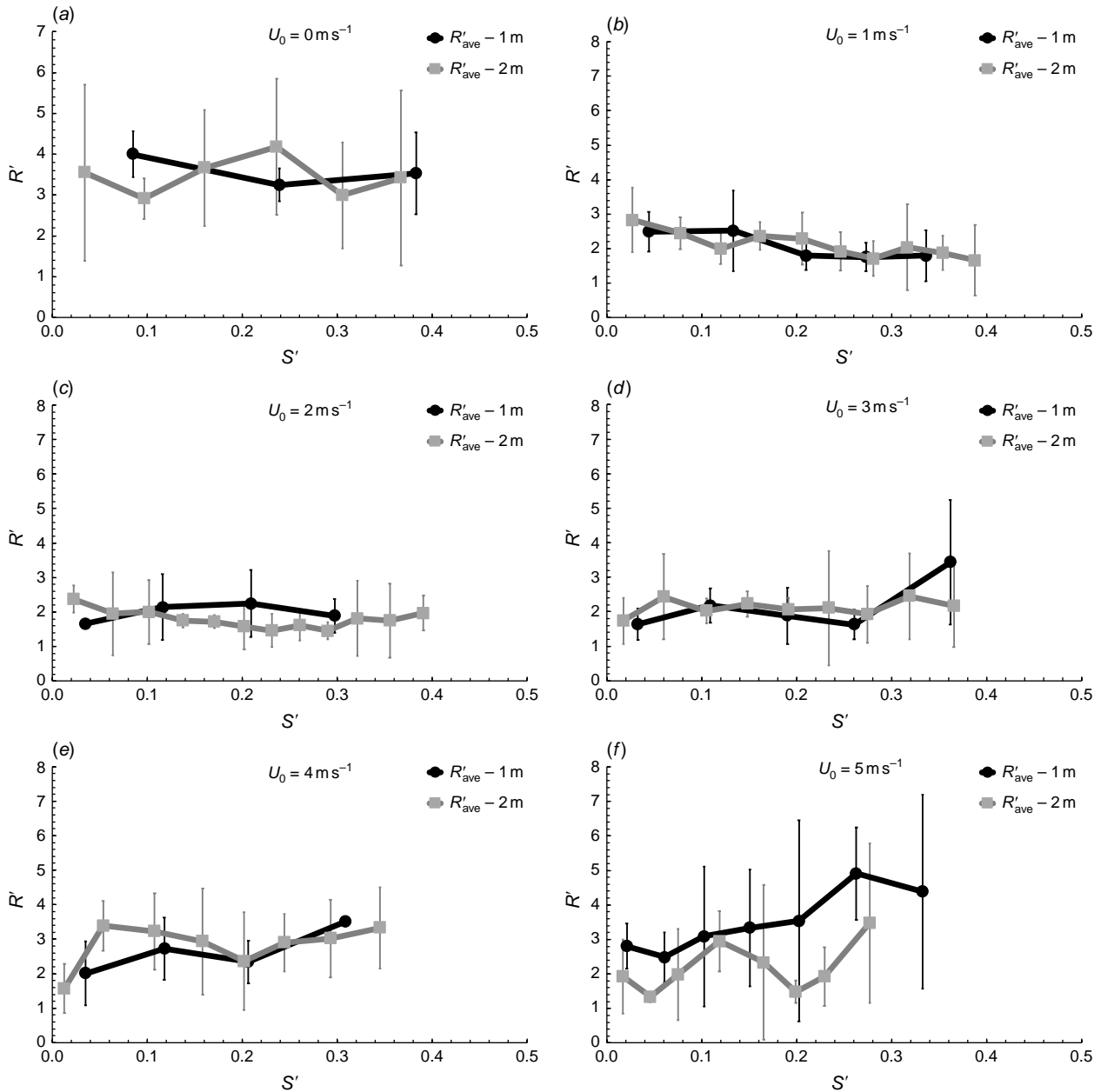


Fig. 6. Non-dimensional ROS between two fire fronts under different wind flow velocities (U) with two different distances ($d = 1$ and 2 m) as a function of the non-dimensional distance S' . The average values R'_{ave} with the 95% confidence intervals are shown in each case. (a) $U = 0 \text{ m s}^{-1}$; (b) $U = 1 \text{ m s}^{-1}$; (c) $U = 2 \text{ m s}^{-1}$; (d) $U = 3 \text{ m s}^{-1}$; (e) $U = 4 \text{ m s}^{-1}$ and (f) $U = 5 \text{ m s}^{-1}$.

are almost vertical, and the buoyancy flow increases compared with the flow influenced by the wind. The ratio between vertical and horizontal forces tends to equilibrium and results in a minimum value of R'_{ave} (Figs 7, 8, respectively). However, for all burn times and distances, the flame height tends to be constant; see Fig. 9.

For $U_0 = 3, 4$ and 5 m s^{-1} (Fig. 6d–f), the approaching velocity R'_{ave} generally tends to increase with the approaching fires, with marked oscillations (Fig. 6f). When $U_0 = 5 \text{ m s}^{-1}$, the non-dimensional ROS in general increases because the

flame depth and the amount of fuel that starts burning increase, influenced by the wind flow blowing between two fire lines. The higher wind speed increases turbulence, a highly important factor, decreasing the flame height, but increasing combustion processes.

Average values

In order to assess the overall role of the parameters d and U in the interaction between the two lines, we estimate the average

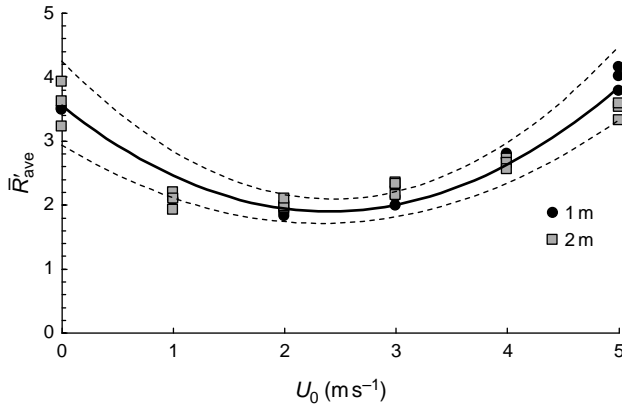


Fig. 7. Average \bar{R}'_{ave} values of three replications performed and two distances $d = 1$ and 2 m as a function of the wind flow velocity U_0 (0 – 5 m s^{-1}). The black curve represents the predicted \bar{R}'_{ave} as function of the wind flow velocity (U_0) defined by Eqn 9 with $R^2 = 0.891$. The dashed line curves represent the $\bar{R}'_{ave} \pm \Delta\bar{R}'_{ave}$, the s.d.

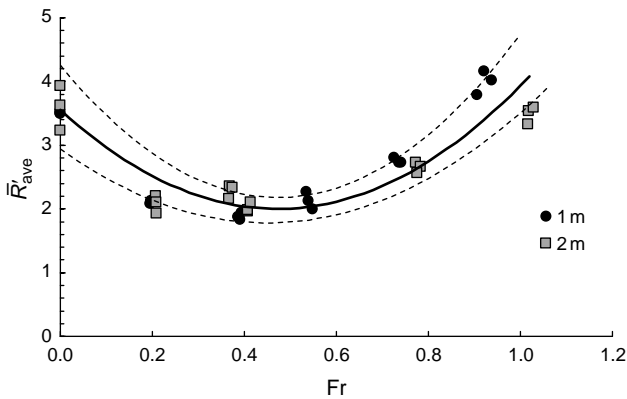


Fig. 8. Average \bar{R}'_{ave} values of three replications performed and two distances $d = 1$ and 2 m as a function of the Froude number (Fr). The black curve represents the predicted \bar{R}'_{ave} as function of the Froude number defined by Eqn 10 with $R^2 = 0.788$. The dashed line curves represent the $\bar{R}'_{ave} \pm \Delta\bar{R}'_{ave}$, the s.d.

\bar{R}'_{ave} values for each reference line and for each distance ($d = 1$ and 2 m). These values are plotted in Fig. 7 as a function of the wind flow velocity U_0 (0 – 5 m s^{-1}) for all tests performed. As can be seen, the values of \bar{R}'_{ave} show a similar trend with a marked minimum for wind velocity between $U_0 = 1$ and 2 m s^{-1} .

The set of data points was fitted by a quadratic law given by:

$$\bar{R}'_{ave} = 0.287U_0^2 - 1.376U_0 + 3550 \quad (9)$$

The correlation coefficient R^2 for this fit is 0.891 . Therefore, we consider that for the present experimental conditions, the non-dimensional ROS is independent of the distance between the fire lines and there is a wind velocity value between 1 and 2 m s^{-1} for which the ROS has an

overall minimum value. Two-way ANOVA with replication indicated that the approaching fire \bar{R}'_{ave} was significantly (P -value < 0.05) affected by the wind flow (U_0), but the distance between two fire lines, for the range of experimental laboratory tests performed, did not significantly affect \bar{R}'_{ave} (P -value > 0.05).

The ratio between the vertical forces induced by the buoyancy flow, which happens during the ascension of the hot gases, and the horizontal forces produced by the wind was calculated, according to Eqn 6. Fig. 8 shows the non-dimensional average \bar{R}'_{ave} plotted as a function of the Froude number (Fr) for all tests performed. As can be seen in Fig. 8, the values of \bar{R}'_{ave} as a function of Fr have a similar trend, with a marked minimum for the same \bar{R}'_{ave} as for $U_0 = 1$ and 2 m s^{-1} . The set of data points was fitted by a quadratic law given by:

$$\bar{R}'_{ave} = 6942Fr^2 - 6559Fr + 3550 \quad (10)$$

The correlation coefficient R^2 for this fit is 0.788 . Therefore, we consider that for the present experimental conditions, the ratio between horizontal and vertical force lines affecting the approaching ROS is independent of the initial distance between the fires. Two-way ANOVA with replication indicated that the Froude number was significantly (P -value < 0.05) affected by the wind flow (U_0), but the distance between the two fire lines for the experimental laboratory tests performed did not significantly (P -value > 0.05) affect the Froude number.

Physical interpretation of fire evolution

Our experiments show that the average rate of lateral spread of two fire lines with parallel wind varies in a non-monotonic way with the wind velocity. In order to interpret this result, which to our knowledge is reported for the first time, we analysed in great detail the videos of these and other similar experiments in combination with the instantaneous values of the ROS to provide an explanation for the existence of a minimum value for the ROS.

We know that fire spread is always three-dimensional and the fluctuations of the fire and flow properties create cells of convection (Finney et al. 2015). In order to simplify our interpretation of the dynamic interaction between the fires, the fuel bed and the surrounding flow, to explain the non-monotonic or intermittent behaviour of fire, according Viegas et al. (2021), we consider the evolution of fire and flame properties along a given reference direction. As we are concerned with the phenomena that occur when two parallel fire lines interact affected by parallel wind flow, we consider a line parallel to the OY axis between the two fire lines.

In Fig. 9, we present a physical interpretation of the fire spread properties for the three values of the flow velocity ($U_0 = 0, 2$ and 5 m s^{-1}) corresponding to the three fire

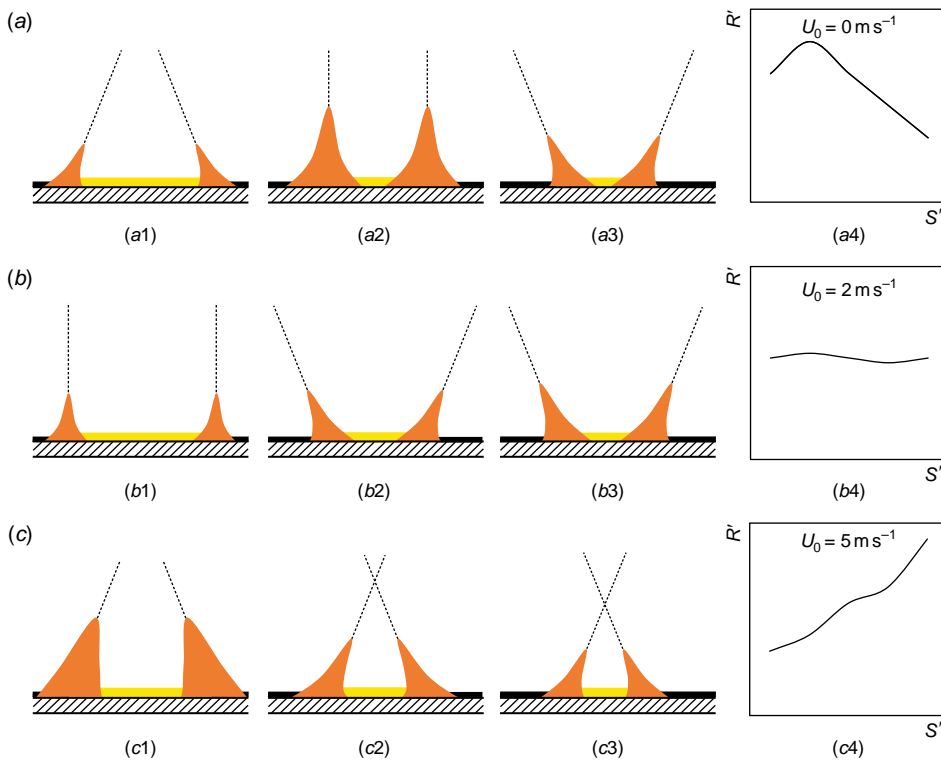


Fig. 9. Physical interpretation of fire evolution of a 2D flame during the integration of the two parallel fire lines for three different wind flow velocities. (a–c) are considered a wind flow U_0 velocity equal to 0, 2 and 5 m s^{-1} , respectively. For each wind velocity, we consider three different stages during the integration of the two parallel fire lines (e.g. stage a1–a4, b4 and c4) represent the conceptual evolution of the non-dimensional ROS towards two fire fronts in function of the time for $U_0 = 0, 2$ and 5 m s^{-1} , respectively.

spread regimes that were identified. For each flow velocity, we show three different stages when the fire fronts spread towards each other. The inset diagram shows the typical evolution of the ROS as a function of the local non-dimensional distance S' between the fire lines, as given in Figs 5, 6.

As shown in each case, the flame geometry and size change during the fire fronts' advance in a way that depends on the flow velocity. These changes are associated with the role of horizontal and vertical forces that change the flame geometry (Morvan 2007; Balbi *et al.* 2020; Viegas *et al.* 2021) and, consequently, the ROS between the two parallel fire lines.

In the absence of wind, $U_0 = 0 \text{ m s}^{-1}$ (Fig. 9a), there is no horizontal flow and buoyancy is the dominating factor. After the two fire lines start to burn, the flames lean towards each other (see Fig. 9a1), and the fire fronts quickly approach each other in this initial phase. After the increase of the burned area by each fire line, the residual heat of the burned area induces an indraft towards the burned areas, the flames become more vertical and the flame length and height increase (see Fig. 9a4). Then, the flames lean towards the burned fuel and spread with decreasing velocity. As the initial stage of acceleration is very strong in this case – absence of horizontal wind – the average ROS is relatively high in spite of the deceleration process that we have during the approach of the two fire lines.

For the wind flow $U_0 = 2 \text{ m s}^{-1}$ (see Fig. 9b), in the first stage (Fig. 9b1), the flame is almost vertical and the

convection flow is symmetrical on both sides of each fire front. In this case, the wind inhibits interaction and the flames are almost vertical. In the second and third stages (see Fig. 9b2, b3), the flames lean towards the burnt area and the flame length and height are constant because the residual heat from the burnt area is dominating the heat from the flames. This leads to stronger flow convergence over the burnt areas. In this case, therefore, most of the time the fire fronts spread as back fires with a relatively low value of ROS. As a consequence, the average value of the ROS is very low compared with the previous case.

For the wind flow $U_0 = 5 \text{ m s}^{-1}$ (see Fig. 9c), the flames of each fire line lean towards each other, the flame angle decreases and the ROS increases during all stages (see Fig. 9c1–c3). As a consequence of this continuous acceleration, for this set of boundary conditions, the average value of ROS is also larger than in the previous case. This can be explained by the effect of the stronger wind intensifying the overall fire behaviour (including the two approaching flanks) and so the heat from the two approaching flame fronts can predominate over the residual heat from the burnt area, leading to stronger flow convergence between the two approaching fire lines. We confirmed the existence of similar behaviour of the fire associated with the typology of the flames and of the convective processes in other types of fires. One of these cases corresponds to the well-controlled experiments of junction fires described in Viegas *et al.* (2021). In their study, strong convective effects were observed during the evolution of fires initiated as two linear

ignition lines intersecting at an angle of 30° and spreading on a slope of 30° . Specifically, near the intersection point, there was a strong convective movement towards the unburned area and a marked acceleration of the fire, while at the other end of the fire line, fire-induced convection inclined the flames towards the burned fuel, therefore reducing the ROS. At other points along the fire line, there was a balance of convection conditions and the ROS remained practically constant during the spread.

Conclusion

The interaction of two parallel fire fronts initially separated by a distance d spreading laterally in a parallel flow under different wind velocities was studied. Our experimental results obtained in a set of test conditions showed that the average ROS of the two approaching fires is independent of the initial distance between the lines but varies non-monotonically with the wind velocity.

In the absence of wind, the average ROS of the two approaching fires has a relatively high value that decreases with increasing wind velocity, reaching a minimum value for a range of relatively low values of wind velocity, and then increases with wind velocity. In the present tests, which were performed for wind velocities up to 5 m s^{-1} , the minimum value of the ROS was obtained for wind velocities between 1 and 2 m s^{-1} .

Based on analysis of the ROS of the fire and of the flame properties during the fire spread, a physical interpretation of the dynamics of fire spread is provided to justify the existence of this minimum value. The balance between fire-induced buoyancy and wind flow determines the angle and length of the flames, causing the fire to spread relatively rapidly in the absence of wind, owing to high initial acceleration. For relatively low values of wind speed, the ROS of the fire lines remains constant and relatively low. With increasing wind velocity, the flames lean towards the unburned fuel between the fire lines, accelerating their spread and increasing the average value of the ROS.

In future work, we intend to analyse in more detail the dynamic evolution of the fire and its interaction with the surrounding flow between the fire lines and the corresponding variation of the values of ROS between two parallel fire lines. The centre of convergence of the pyrogenic flow will be analysed and compared with numerical simulations. This will be performed for a wider range of laboratory experiments (with wind flow or slope influence) with standard fuel bed types and field experiments. To better compare with wildfire situations, it is also important to increase the scale factor of the dimension of the fire line length and of the distance between fire lines. Development of a mathematical model to interpret the present results and its application to the analysis of real fires will be addressed in future work.

Symbols

h_f	Fuel bed height
β_f	Packing ratio
ρ_b	Fuel bed bulk density
ρ_p	Particle density
σ_f	Particle surface-area-to-volume ratio
B_{ij}	Width of burned area
c_i	Shape coefficient
S	Distances travelled by the fire line from the origin
P	Generic point of coordinates (x, y, z)
x	Coordinate along the fire spread (cm)
y	Transverse horizontal coordinate (cm)
z	Vertical coordinate (cm)
d	Distance between fire fronts (m)
m_f	Moisture content of the fuel bed particles (dry basis)
U_0	Flow velocity vector (m s^{-1})
R	Rate of spread (ROS) (cm s^{-1})
R_0	Basic rate of spread (cm s^{-1})
R'	Non-dimensional ROS
l_1	Fire front 2 m long defined by straight line KL
l_2	Fire front 2 m long defined by straight line IJ
t_i	Time of measurement (s)
t_j	Average time between two consecutive measurements (s)
P_i	Average of the positions of each fire front (l_1 and l_2), $P_{1,i}(S_i, t_i)$ and $P_{2,i}(S_i, t_i)$
ΔS_i	Distance variation of the positions of fire between $P_i(S_i, t_i)$ and $P_{i+1}(S_{i+1}, t_{i+1})$ at predefined times (i)
S'	Non-dimensional distance
g	Acceleration due to gravity (m s^{-2})
Fr	Froude number

References

- Águeda A, Pastor E, Pérez Y, Viegas DX, Planas E (2011) Fire intensity reduction in straw fuel beds treated with a long-term retardant. *Fire Safety Journal* **46**, 41–47. doi:10.1016/j.firesaf.2010.11.003
- Alexander ME, Cruz MG (2013) Assessing the effect of foliar moisture on the spread rate of crown fires. *International Journal of Wildland Fire* **22**, 415–427. doi:10.1071/WF12008
- Almeida MA de FB de (2005) Caracterização da combustibilidade de leitões florestais heterogêneos. Master's thesis. Universidade de Aveiro, Aveiro, Portugal. Available at <http://hdl.handle.net/10773/4597>
- Balbi JH, Chatelon FJ, Morvan D, Rossi JL, Marcelli T, Morandini F (2020) A convective–radiative propagation model for wildland fires. *International Journal of Wildland Fire* **29**, 723–738. doi:10.1071/WF19103
- Bowman DMJS, Williamson GJ, Abatzoglou JT, Kolden CA, Cochrane MA, Smith AMS (2017) Human exposure and sensitivity to globally extreme wildfire events. *Nature Ecology and Evolution* **1**, 0058. doi:10.1038/s41559-016-0058
- Brown AA, Davis K (1973) 'Forest Fire – Control and Use.' (McGraw-Hill: New York, NY, USA)
- Catchpole EA, Catchpole WR, Rothermel RC (1993) Fire behavior experiments in mixed fuel complexes. *International Journal of Wildland Fire* **3**, 45–57. doi:10.1071/WF9930045
- Catchpole EA, Catchpole WR, Viney NR, McCaw WL, Marsden-Smedley JB (2001) Estimating fuel response time and predicting fuel moisture content from field data. *International Journal of Wildland Fire* **10**, 215–222. doi:10.1071/WF01011

- Clark TL, Jenkins MA, Coen J, Packham D (1996) A coupled atmosphere–fire model: convective feedback on fire-line dynamics. *Journal of Applied Meteorology* **35**, 875–901. doi:10.1175/1520-0450(1996)035<0875:ACAMCF>2.0.CO;2
- Devore JL (2010) ‘Probability and Statistics for Engineering and the Sciences’. (Brooks/Cole: Boston, MA, USA)
- Dlugogorski BZ, Hirunpraditkoon S, Kennedy EM (2014) Ignition temperature and surface emissivity of heterogeneous loosely packed materials from pyrometric measurements. *Fire Safety Science* **11**, 262–275. doi:10.3801/IAFSS.FSS.11-262
- Filkov A, Cirulis B, Penman T (2020) Quantifying merging fire behaviour phenomena using unmanned aerial vehicle technology. *International Journal of Wildland Fire* **30**, 197–214. doi:10.1071/WF20088
- Finney MA, Cohen JD, Forthofer JM, McAllister SS, Gollner MJ, Gorham DJ, Saito K, Akafuah NK, Adam BA, English JD (2015) Role of buoyant flame dynamics in wildfire spread. *Proceedings of the National Academy of Sciences* **112**, 9833–9838. doi:10.1073/pnas.1504498112
- Johansen RW (1984) Prescribed burning with spot fires in the Georgia Coastal Plain. *Georgia Forestry Commission* **49**, 1–8. <http://www.treesearch.fs.fed.us/pubs/36481>.
- Lopes S, Viegas DX, Teixeira de Lemos L, Viegas MT (2014) Equilibrium moisture content and timelag of dead *Pinus pinaster* needles. *International Journal of Wildland Fire* **23**, 721. doi:10.1071/WF13084
- Martins Fernandes PA (2001) Fire spread prediction in shrub fuels in Portugal. *Forest Ecology and Management* **144**, 67–74. doi:10.1016/S0378-1127(00)00363-7
- Morvan D (2007) A numerical study of flame geometry and potential for crown fire initiation for a wildfire propagating through shrub fuel. *International Journal of Wildland Fire* **16**, 511–518. doi:10.1071/WF06010
- Morvan D, Meradji S, Mell WE (2011) Numerical study of the interaction between a head and a backfire propagating in grassland. *Fire Safety Science* **10**, 459–470. doi:10.3801/IAF
- Pastor E, Zárate L, Planas E, Arnaldos J (2003) Mathematical models and calculation systems for the study of wildland fire behaviour. *Progress in Energy and Combustion Science* **29**, 139–153. doi:10.1016/S0360-1285(03)00017-0
- Pyne SJ (1984) ‘Introduction to Wildland Fire: Fire Management in the United States.’ (John Wiley and Sons: New York, NY, USA)
- Raposo JR, Cabiddu S, Viegas DX, Salis M, Sharples J (2015) Experimental analysis of fire spread across a two-dimensional ridge under wind conditions. *International Journal of Wildland Fire* **24**, 1008. doi:10.1071/WF14150
- Raposo JR, Viegas DX, Xie X, Almeida M, Figueiredo AR, Porto L, Sharples J (2018) Analysis of the physical processes associated with junction fires at laboratory and field scales. *International Journal of Wildland Fire* **27**, 52–68. doi:10.1071/WF16173
- Raposo JRN (2016) Extreme fire behaviour associated with merging of two linear fire fronts. PhD Thesis, Universidade de Coimbra, Coimbra, Portugal. Available at <http://hdl.handle.net/10316/31020>
- Rodrigues A, Ribeiro C, Raposo J, Viegas DX, André J (2019) Effect of canyons on a fire propagating laterally over slopes. *Frontiers in Mechanical Engineering* **5**, 402–409. doi:10.14195/978-989-26-16-506_43
- Sharples JJ, Towers IN, Wheeler G, Wheeler V, McCoy JA (2013) Modelling fire line merging using plane curvature flow. In ‘20th International Congress on Modelling and Simulation, 1–6 December 2013, Adelaide, Australia’. (Eds J Piantadosi, RS Anderssen, J Boland) pp. 256–262. (The Modelling and Simulation Society of Australia and New Zealand.) Available at <https://www.mssanz.org.au/modsim2013/A3/sharples2.pdf>
- Sullivan AL (2007) Convective Froude number and Byram’s energy criterion of Australian experimental grassland fires. *Proceedings of the Combustion Institute* **31**(II), 2557–2564. doi:10.1016/j.proci.2006.07.053
- Sullivan AL (2009) Wildland surface fire spread modelling, 1990–2007. 3: Simulation and mathematical analogue models. *International Journal of Wildland Fire* **18**, 387. doi:10.1071/WF06144
- Sullivan AL, Swedosh W, Hurley RJ, Sharples JJ, Hilton JR (2019) Investigation of the effects of interactions of intersecting oblique fire lines, with and without wind, in a combustion wind tunnel. *International Journal of Wildland Fire* **28**, 704–719. doi:10.1071/WF18217
- Thomas CM, Sharples JJ, Evans JP (2017) Modelling the dynamic behaviour of junction fires with a coupled atmosphere–fire model. *International Journal of Wildland Fire* **26**, 331–344. doi:10.1071/WF16079
- Viegas DX (2006) Parametric study of an eruptive fire behaviour model. *International Journal of Wildland Fire* **15**, 169–177. doi:10.1071/WF05050
- Viegas DX, Pita LP (2004) Fire spread in canyons. *International Journal of Wildland Fire* **13**, 253–274. doi:10.1071/WF03050
- Viegas DX, Raposo JR, Davim DA, Rossa CG (2012) Study of the jump fire produced by the interaction of two oblique fire fronts. Part 1. Analytical model and validation with no-slope laboratory experiments. *International Journal of Wildland Fire* **21**, 843–856. doi:10.1071/WF10155
- Viegas D, Raposo J, Figueiredo A (2013a) Preliminary analysis of slope and fuel bed effect on jump behavior in forest fires. *Procedia Engineering* **62**, 1032–1039. doi:10.1016/j.proeng.2013.08.158
- Viegas DX, Soares J, Almeida M (2013b) Combustibility of a mixture of live and dead fuel components. *International Journal of Wildland Fire* **22**, 992–1002. doi:10.1071/WF12031
- Viegas DX, Almeida MA, Ribeiro LM, Raposo J, Viegas MT, Oliveira R, Alves D, Pinto C, Rodrigues A, Ribeiro C, Lopes S, Jorge H, Viegas CX (2019) ‘Análise dos Incêndios Florestais Ocorridos a 15 de outubro de 2017.’ (Centro de Estudos sobre Incêndios Florestais (CEIF/ADAI/LAETA))
- Viegas DXFC, Raposo JRN, Ribeiro CFM, Reis LCD, Abouali A, Viegas CXP (2021) On the non-monotonic behaviour of fire spread. *International Journal of Wildland Fire* **30**, 702–719. doi:10.1071/WF21016
- Xie X, Liu N, Viegas DX, Raposo JR (2014) Experimental research on upslope fire and jump fire. *Fire Safety Science* **11**, 1430–1442. doi:10.3801/IAFSS.FSS.11-1430
- Xie X, Liu N, Raposo JR, Viegas DX, Yuan X, Tu R (2020) An experimental and analytical investigation of canyon fire spread. *Combustion and Flame* **212**, 367–376. doi:10.1016/j.combustflame.2019.11.004

Data availability. Data are available only under request to the corresponding author: Carlos Ribeiro, carlos.ribeiro@adai.pt.

Conflicts of interest. The authors declare no conflict of interest.

Declaration of funding. The work reported in this article was carried out under the scope of projects Firestorm (PCIF/GFC/0109/2017), McFire (PCIF/MPG/0108/2017), IMfire (PCIF/SSI/0151/2018), SmokeStorm (PCIF/MPG/0147/2019) and SafeFire (PCIF/SSO/0163/2019), supported by the Portuguese National Science Foundation, Region (Centro 2020, Centro-01-0246-FEDER-000015) and European Union’s Horizon 2020 research and innovation programme under grant agreement No. 101003890, FirEUrisk – Developing A Holistic, Risk-Wise Strategy For European Wildfire Management. We thank the FCT Foundation for Science and Technology for the PhD grants of Carlos Ribeiro and André Rodrigues with references SFRH/BD/140923/2018 and SFRH/BD/138235/2018, respectively.

Acknowledgements. The support given by Nuno Luís and Gonçalo Rosa in performing the laboratory experiments is gratefully acknowledged. Luis Mário Ribeiro and Tiago Rodrigues are thanked for collaboration with some images and statistical analysis, respectively.

Author contributions. Conceptualisation: CR, JR and DXV; data curation: CR and BS; formal analysis: CR, BS and JR; methodology: CR, JR, LR and DXV; experimental test: CR, BS, LR, JR and AR; supervision: JR and DXV; writing – original draft: CR; writing – review and editing – CR, LR, JR, AR, DXV and JS.

Author affiliations

^AUniv Coimbra, ADAI, Departamento de Engenharia Mecânica, Rua Luís Reis Santos, Pólo II, 3030-788 Coimbra, Portugal.

^BSchool of Science, University of New South Wales (UNSW), Canberra, ACT, Australia.

^CBushfire and Natural Hazards Cooperative Research Centre, East Melbourne, Vic., Australia.

Appendix I. Laboratory experiments

Laboratory experiments were carried out at the Forest Fire Research Laboratory of the University of Coimbra using an indoor CT. The fuel used in all tests was composed of dry particles of straw (*Avena sativa*) with a constant load of 600 g m^{-2} (dry basis). Inside the CT, the wind velocity was measured for wind velocities 1, 3 and 5 m s^{-1} in the OX axis at points $P_{x,y}$ where x and y are the coordinates relative to the referential OXY, with a KimoAMI 300 hot-wire probe 22 cm above the CT ground (OZ axis). Fig. A1a shows the positions where flow velocity was measured.

The values presented in Tables A1–A3 corresponds to the wind velocity values U_0 of 1, 3 and 5 m s^{-1} , respectively. In order to reduce uncertainty, three measurements (M1, M2 and M3) were performed for each set of parameters during 30 s for each position.

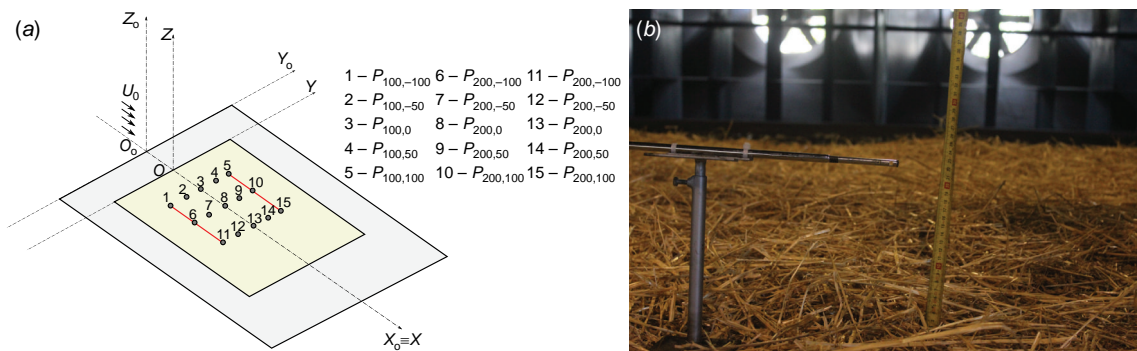


Fig. A1. (a) Distribution of points $P_{x,y,z}$ where wind velocity was measured for wind velocities 1, 3 and 5 m s^{-1} in the OX axis. (b) KimoAMI 300 hot-wire probe (Kimo Instruments, Montpon-Ménéstérol, France), 22 cm above the CT ground (OZ axis).

Table A1. Wind velocity for $U_0 = 1 \text{ m s}^{-1}$.

X	Y	M1				M2				M3			
		Min.	Max.	Avg	Dev.	Min.	Max.	Avg	Dev.	Min.	Max.	Avg	Dev.
100	-100	0.98	1.12	1.04	0.05	0.79	1.10	1.01	0.08	0.82	0.95	0.89	0.04
100	-50	1.22	1.46	1.34	0.09	1.18	1.52	1.37	0.10	1.24	1.51	1.35	0.11
100	0	1.07	1.48	1.29	0.12	1.19	1.38	1.29	0.06	1.22	1.43	1.30	0.07
100	50	0.86	1.31	1.09	0.14	1.01	1.68	1.34	0.19	1.15	1.47	1.32	0.11
100	100	0.96	1.41	1.16	0.14	1.06	1.47	1.26	0.13	0.83	1.20	1.01	0.11
200	-100	1.05	1.23	1.13	0.06	0.92	1.25	1.10	0.10	0.95	1.32	1.10	0.13
200	-50	0.90	1.37	1.10	0.15	1.15	1.35	1.24	0.07	0.86	1.50	1.14	0.27
200	0	0.80	1.80	1.90	0.21	1.19	1.65	1.37	0.18	0.98	1.29	1.10	0.09
200	50	1.20	1.39	1.24	0.06	0.95	1.30	1.11	0.14	1.16	1.41	1.24	0.08
200	100	0.97	1.50	1.18	0.25	0.96	0.96	0.91	0.04	0.73	0.98	0.81	0.06
300	-100	0.84	1.15	0.97	0.09	0.88	1.00	0.93	0.03	0.89	1.22	1.06	0.11
300	-50	1.04	1.61	1.23	0.16	0.97	1.75	1.26	0.27	0.93	1.22	1.00	0.08
300	0	1.11	1.46	1.23	0.09	0.96	1.51	1.19	0.15	1.00	1.21	1.01	0.06
300	50	0.75	1.09	0.92	0.11	0.76	0.98	0.88	0.07	0.85	1.09	0.96	0.08
300	100	0.88	1.30	1.04	0.11	0.69	1.05	0.85	0.09	0.88	1.08	0.96	0.06

Table A2. Wind velocity for $U_0 = 3 \text{ m s}^{-1}$.

X	Y	M1				M2				M3			
		Min.	Max.	Avg	Dev.	Min.	Max.	Avg	Dev.	Min.	Max.	Avg	Dev.
100	-100	2.60	3.87	3.279	0.40	2.67	3.46	3.12	0.28	2.7	4.32	3.50	0.52
100	-50	3.10	4.60	3.57	0.48	2.84	4.15	3.66	0.49	3.4	3.80	3.63	0.15
100	0	3.30	4.90	4.00	0.48	3.10	4.20	3.91	0.27	3.4	4.80	4.09	0.50
100	50	2.67	4.11	3.28	0.52	2.25	4.16	3.26	0.54	3.1	3.90	3.41	0.28
100	100	2.51	3.60	3.01	0.30	2.62	4.05	3.15	0.43	2.06	3.23	2.70	0.36
200	-100	3.10	4.50	3.75	0.43	3.10	3.70	3.28	0.18	2.73	3.62	3.29	0.32
200	-50	3.00	4.60	3.20	0.46	2.77	4.76	3.63	0.55	4.00	5.00	4.49	0.34
200	0	3.20	4.20	3.64	0.32	3.30	4.30	3.94	0.33	3.40	4.40	3.83	0.28
200	50	2.88	3.49	3.24	0.16	2.59	3.64	3.01	0.37	2.76	4.30	3.39	0.46
200	100	2.86	3.31	3.07	0.15	2.63	3.99	3.23	0.47	2.75	3.93	3.21	0.35
300	-100	2.70	3.35	3.02	0.22	2.70	4.09	3.49	0.36	3.00	3.80	3.54	0.20
300	-50	3.40	5.00	4.27	0.57	3.40	4.80	4.02	0.41	3.40	5.30	4.28	0.66
300	0	3.50	4.30	3.96	0.29	3.00	4.10	3.54	0.29	2.79	4.03	3.54	0.41
300	0.5	2.25	3.92	3.19	0.52	2.70	4.00	3.40	0.45	2.50	3.60	3.17	0.29
300	1	2.22	3.62	2.92	0.37	2.70	3.19	3.01	0.12	2.65	3.57	3.00	0.27

Table A3. Wind velocity for $U_0 = 5 \text{ m s}^{-1}$.

X	Y	M1				M2				M3			
		Min.	Max.	Avg	Dev.	Min.	Max.	Avg	Dev.	Min.	Max.	Avg	Dev.
100	-100	4.6	5.7	5.14	0.38	4.99	5.21	5.10	0.43	4.99	5.21	5.10	0.70
100	-50	5.0	7.4	6.26	0.81	4.93	6.72	5.82	0.44	4.93	6.72	5.82	1.56
100	0	5.1	6.7	6.04	0.40	5.48	6.98	6.23	0.33	5.48	6.98	6.23	0.36
100	50	3.5	6.2	4.86	0.99	3.89	6.09	4.99	0.51	3.89	6.09	4.99	0.64
100	100	4.2	5.8	4.89	0.58	4.05	6.58	5.32	0.27	4.05	6.58	5.32	0.27
200	-100	4.3	5.9	5.18	0.44	4.38	5.63	5.00	0.70	4.38	5.63	5.00	0.43
200	-50	4.3	8.0	5.78	1.05	4.98	7.44	6.21	1.56	4.98	7.44	6.21	0.44
200	0	4.8	6.0	5.38	0.37	4.26	5.51	4.89	0.36	4.26	5.51	4.89	0.33
200	50	4.4	6.4	5.4	0.49	4.68	6.38	5.53	0.64	4.68	6.38	5.53	0.51
200	100	4.0	4.9	4.51	0.27	4.09	5.58	4.84	0.27	4.09	5.58	4.84	0.27
300	-100	4.8	6.3	5.51	0.43	4.99	6.28	5.63	0.38	4.99	6.28	5.63	0.38
300	-50	5.7	7.1	6.27	0.44	5.60	7.16	6.38	0.81	5.60	7.16	6.38	0.81
300	0	5.5	6.7	5.98	0.33	5.43	7.22	6.33	0.40	5.43	7.22	6.33	0.40
300	50	3.8	5.5	4.96	0.51	4.42	5.64	5.03	0.99	4.42	5.64	5.03	0.99
300	100	3.9	4.7	4.46	0.27	3.68	4.10	3.89	0.58	3.68	4.10	3.89	0.58